JOURNAL OF GUIDANCE, CONTROL, AND DYNAMICS
Vol. 22, No. 1, January–February 1999

Autonomous Maneuver Tracking for Self-Piloted Vehicles

David P. Boyle*
University of Sydney, Sydney, New South Wales 2006, Australia
and
Gregory E. Chamitoff†
NASA Johnson Space Center, Houston, Texas 77058

A fully autonomous flight vehicle must be capable of accurately tracking a desired trajectory for the safe and effective completion of a given mission. An approach to maneuver autopilot design is presented based on a six-degree-of-freedom nonlinear trimming algorithm coupled with a robust tracking controller. Acceleration commands required for closed-loop tracking of a desired trajectory in an Earth-fixed reference frame are provided by a simple guidance strategy. The trimming algorithm generates optimal state commands and feedforward controls to accomplish the maneuver, while assuring that these commands can be tracked by an inner-loop controller without violating vehicle performance or actuator constraints. This approach is demonstrated in simulated flight of an actual fixed-wing uninhabited aerial vehicle, named *Ariel*. Excellent tracking performance is achieved for a representative three-dimensional trajectory using a high-fidelity aircraft model with nonlinear dynamics and realistic wind gust disturbances. In addition, an analysis of system robustness to uncertainty in the vehicle model is performed.

I. Introduction

A LOW-COST, fixed-wing uninhabited aerial vehicle (UAV) named *Ariel* has been designed, built, and flown by the Department of Aeronautical Engineering, University of Sydney. The UAV has a mass of 32.5 kg, and 3.02-m wingspan. The objective of flight control research is to transform the UAV into a self-piloted vehicle through development of onboard mission planning, trajectory optimization, and robust maneuver tracking control functions.

Among other applications, an important use for UAVs is subscale (or full-scale) flight testing and analysis, especially in conditions characterized by time-varying and highly nonlinear dynamics. High-precision and robust flight control systems could perform required flight-test maneuvers with accuracy, repeatability, economy, and safety. Robust maneuver tracking is also highly desirable in current applications, where the optimal use of vehicle capabilities is essential to mission success or perhaps survivability. These considerations motivate the development of a new approach for high-performance maneuver control in autonomous flight vehicles.

The problem of controlling an aircraft to track a desired trajectory has been approached a number of different ways in the literature. In Ref. 1, e.g., multiple interconnected classical control loops were used to track commanded states. This general approach has been widely used, but is only useful to obtain limited performance over a restricted flight envelope. Fine tuning of controller gains is required, and there is no means for optimizing performance or characterizing robustness.

Another general approach can be classified as prediction-based algorithms. These methods determine a feedforward control solution to accomplish a desired maneuver based on an internal model of the aircraft dynamics. A numerical approach, called inverse simulation, has been applied successfully to aircraft control problems.[2,3] This is essentially an iterative algorithm that repetitively performs stepwise dynamic simulations. It does not, however, account for model uncertainty. A related, but more rigorous approach[4] solves a receding horizon optimal control problem for each stepwise control input. The system, though, is limited to linear dynamics, and again the uncertainty in predictions of aircraft response is not directly addressed.

More recently, nonlinear control techniques have been applied to the aircraft tracking problem. Both Refs. 5 and 6 present strategies that combine input/output linearization with classical proportional integral derivative control in outer command loops to obtain good performance over an expanded flight envelope and stability robustness to modeling errors. This also requires complex gain tuning when applied to the full multivariable tracking problem. In addition, robustness qualities cannot easily be related to specific parameter uncertainties. This problem is addressed formally in Ref. 7, where plant uncertainties are handled by a robust version of the input/output linearization technique. Restrictions on the plant, however, such as being affine in the controls and minimum phase, are difficult to satisfy with typical aircraft dynamics. Nevertheless, these techniques could provide robust inner loops for the maneuver tracking approach considered here.

Successful trajectory control and maneuver modeling techniques have also been developed based on singular perturbation theory[8] and minimum error excitation.[9] However, these techniques require the generation of complete commanded state and control histories for a given maneuver, as opposed to utilizing a desired trajectory in inertial space only. Optimal control for desired outputs[10] also requires an a priori definition of output history required for given trajectories.

This paper presents an autonomous flight control strategy capable of high-performance tracking of a given three-dimensional Earth-fixed flight trajectory in the presence of nonlinear dynamics and parameter uncertainty. This is achieved by dividing the control task into three parts, a simple three-dimensional guidance loop, a six-degree-of-freedom (DOF) feedforward maneuver control law, and a robust inner-loop command-following controller. An advantage of this separation, and important to the approach presented here, is that the vehicle performance and control constraints, as well as dynamic nonlinearities, are handled by the maneuver logic, while the inner-loop controller accounts for parametric uncertainty. The vehicle model uses tabulated aircraft stability and control derivatives. As such, it cannot be inverted in closed form to compute desired control input histories for a nominal trajectory (as in many other algorithms). The essential component of this design is a 6-DOF nonlinear trimming algorithm that determines optimal state and feedforward control commands based on a search procedure that achieves optimal vehicle accelerations without violating performance or actuator limitations. Commanded accelerations are obtained from filtered trajectory errors and their derivatives, and 6-DOF maneuver commands are followed by an inner-loop controller that is designed for robustness to expected parameter uncertainty.

The approach is similar to that of Refs. 11 and 12. Unlike these methods though, the technique presented here does not rely on

Received July 21, 1997; revision received July 13, 1998; accepted for publication July 16, 1998.

*Associate Lecturer, Department of Aeronautical Engineering. Member AIAA.

†Flight Controller–Lead Engineer, Guidance, Navigation, and Control Branch, United Space Alliance, 2101 NASA Rd. 1, MC-DF64. Senior Member AIAA.

separation of force and moment dynamics for decoupling of trim calculations. It also incorporates nonzero body rate commands, which provides for a unique, quasitrimmed solution for aircraft states and controls. Another similar trimming function is presented in Ref. 13 for retrimming an aircraft after structural or control failures. In contrast, the algorithm here is used for maneuver tracking and is not limited to linear systems or equilibrium flight conditions. The approach here is based on an iterative search procedure using a complete nonlinear model of the aircraft. This procedure identifies the optimal solution from the set of feasible maneuvers with respect to the constraints.

The maneuver tracking control system is a subset of a complete autonomous guidance and control system under development for UAV *Ariel*. A brief overview of the complete system is given to indicate the context for the contributions of this research. The maneuver tracking problem is then defined, and the 6-DOF nonlinear maneuver algorithm is discussed in detail. The approach used for inner-loop control is presented, and robustness to parametric uncertainty is analyzed. Finally, the complete system performance is demonstrated for a simulated maneuver sequence.

II. Autonomous Flight Control System

The autonomous flight control system is shown in Fig. 1. The UAV vehicle dynamics are represented by a nonlinear model, a low-altitude gust model, and realistic sensor models. This provides a high-fidelity simulation of the vehicle behavior and is used to evaluate the performance of the flight control system.

Autonomous guidance is provided largely by an optimized flight-path generation routine. It calculates the current optimal three-dimensional trajectory, accounting for geometric constraints (obstacles) and aircraft performance limitations. This capability has been developed through a parallel research effort and is not the focus of this paper. Details can be found in Refs. 14–16. Of importance is simply that the desired position, velocity, and acceleration is provided, at any given time, in an Earth-fixed reference frame.

A guidance computer is used to generate the local trajectory commands that will be followed by the maneuver tracking system. This function provides a smoothly converging path from off-track flight conditions (which will occur due to wind gusts, sensor noise, and model uncertainty). The guidance computer directly generates desired vehicle accelerations, which provide exponentially asymptotic convergence to the optimized flight path.

The 6-DOF maneuver autopilot, which is the focus of this paper, is an optimal trimming function that determines stepwise vehicle attitude and control inputs to track a commanded acceleration in the presence of constraints on the states and controls. It, thus, provides the interface between the desired trajectory in an Earth-fixed frame and the maneuver required by the aircraft to track the flight path. Feedforward control commands are generated, such that the vehicle would perfectly track a feasible path in the absence of modeling errors and disturbances.

An extended Kalman filter will be used to update full-state estimates based on the fusion of data from multiple sensors.

Finally, a robust tracking controller routine provides inner-loop feedback. The controller's outputs are combined with feedforward controls from the maneuver autopilot. A linear quadratic tracking design is used, and the effect of parametric uncertainty is analyzed.

III. 6-DOF Maneuver Logic

The objective of the 6-DOF maneuver algorithm is to determine the optimal and feasible single-step commanded vehicle states and controls required to track the desired trajectory. The solution procedure uses a novel search strategy to determine the best admissible instantaneous flight condition. Search direction is based on the achievable acceleration for a given state vector. Constraints include nonlinear dynamics, vehicle performance, and control actuator limitations. A unique solution is identified by constraining the DOFs to a feasible subset of the state and control space derived from physical considerations of the aircraft control problem.

A. Aircraft Dynamic Equations

The true motion of an aircraft is described (neglecting disturbances) by nonlinear differential equations, which may be written in terms of translational and rotational dynamics (see Ref. 17).

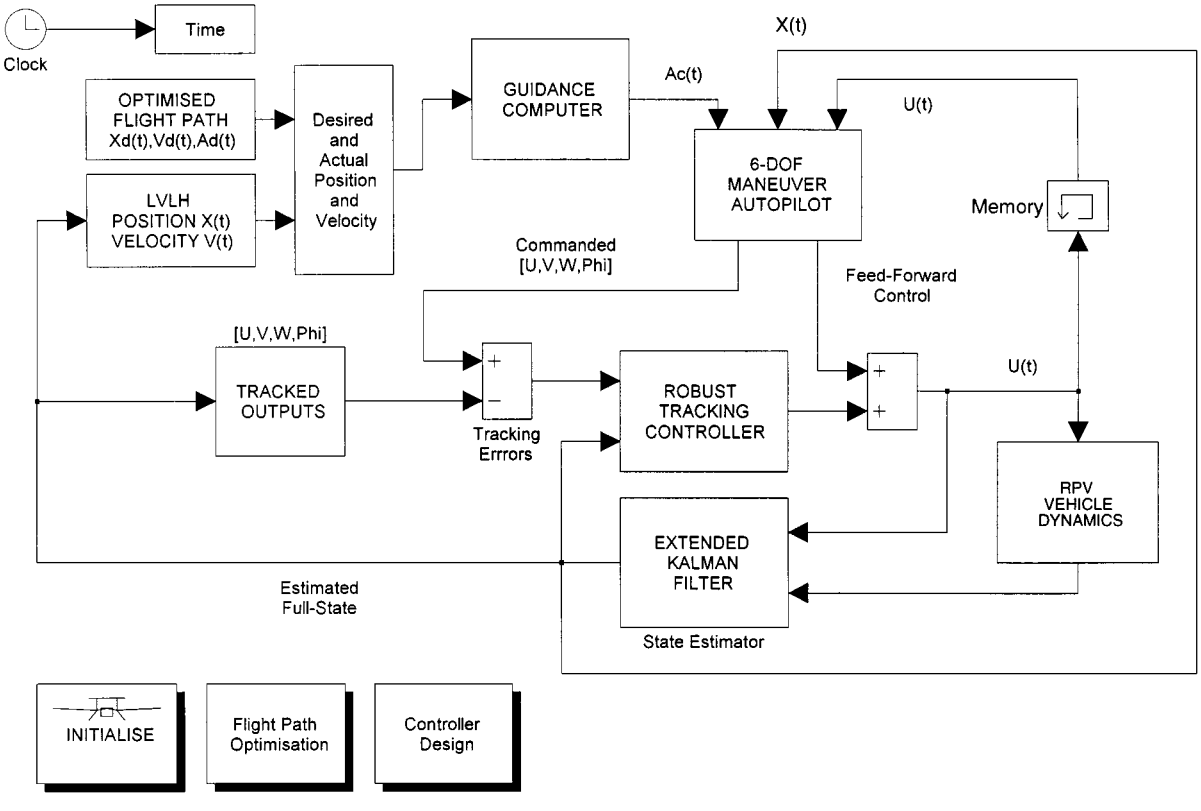

Fig. 1 Complete autonomous flight control system.

The translational (force) dynamics in a wind-axis coordinate system are given by

$$X_W - mg\sin\theta_W = m\dot{V}, \qquad Y_W + mg\cos\theta_W\sin\phi_W = mVr_W$$
$$Z_W + mg\cos\theta_W\cos\phi_W = -mVq_W \tag{1}$$

where X_W, Y_W, and Z_W are the wind-axis components of the aerodynamic and propulsive forces acting on the aircraft; V is the total velocity; ϕ_W, θ_W, and ψ_W are the wind-axis attitude angles; q_W and r_W are the wind-axis pitch and yaw rates; and m is the aircraft mass.

The rotational (moment) dynamics in body-axis coordinates are given by

$$L = I_{xx}\dot{p} - I_{xz}(\dot{r} + pq) - (I_{yy} - I_{zz})qr$$
$$M = I_{yy}\dot{q} - I_{xz}(r^2 - p^2) - (I_{zz} - I_{xx})rp \tag{2}$$
$$N = I_{zz}\dot{r} - I_{xz}(\dot{p} - qr) - (I_{xx} - I_{yy})pq$$

where L, M, and N and p, q, and r are moment and angular velocity components, respectively, about the x, y, and z body axes and I_{ij} are the mass moments of inertia. Note aircraft symmetry about the x–z plane is assumed.

The forces X_W, Y_W, and Z_W and moments L, M, and N in Eqs. (1) and (2), and thus the aircraft's acceleration, are functions of the body-axis defined aircraft states $\boldsymbol{x} = [u, w, q, \theta, h, v, p, r, \phi, \psi]^T$, i.e., x-wise body axis velocity, z-wise body axis velocity, pitch rate, pitch angle, altitude, y-wise body axis velocity, roll rate, yaw rate, roll angle, and azimuth angle, respectively, and controls $\boldsymbol{u} = [\delta_e, \delta_t, \delta_a, \delta_r]^T$, i.e., elevator deflection, throttle setting (percentage power), aileron deflection, and rudder deflection, respectively. The relationship itself is given in Sec. III.C [see Eq. (7)].

B. Problem Statement

Given the aircraft's state and desired acceleration in the local vertical local horizontal (LVLH) frame ($\boldsymbol{a}_{d_{\text{LVLH}}} = [a_{x_d}, a_{y_d}, a_{z_d}]^T_{\text{LVLH}}$), the function of the 6-DOF trimming algorithm is to calculate the states $\boldsymbol{x}$ and controls $\boldsymbol{u}$ that minimize the 2-norm of the difference between the achievable acceleration $\boldsymbol{a}_{a_{\text{LVLH}}} = [a_{x_a}, a_{y_a}, a_{z_a}]^T_{\text{LVLH}}$ and the desired acceleration $\boldsymbol{a}_{d_{\text{LVLH}}}$. That is,

$$\min_{(\boldsymbol{x}\in\boldsymbol{X},\boldsymbol{u}\in\boldsymbol{U})} \left\| \boldsymbol{a}_{d_{\text{LVLH}}} - \boldsymbol{a}_{a_{\text{LVLH}}}(\boldsymbol{x},\boldsymbol{u}) \right\|_2$$

subject to the constraint that

$$(\boldsymbol{X},\boldsymbol{U}) = \{(\boldsymbol{x},\boldsymbol{u}) : \boldsymbol{x} \text{ and } \boldsymbol{u} \text{ are feasible}\} \tag{3}$$

That is, the objective is to find the best possible orientation for the aircraft such that it will achieve (or will be as close as possible to achieving) some desired overall acceleration. The control inputs required for this orientation must also be provided. This must be done in a realistic, feasible manner, subject to constraints on the allowable values for $\boldsymbol{x}$ and $\boldsymbol{u}$. Restrictions on $\boldsymbol{x}$ include angle-of-attack limits, attitude restrictions, and performance restrictions, such as maximum turn rate. Maximum allowable control surface deflections and rates and power limitations form the restrictions on $\boldsymbol{u}$.

C. Solution Concept: Quasitrimmed Flight Condition

There are enough DOFs that the solution of the minimization problem (3) for the states and controls, while meeting the constraints imposed by the dynamics (1) and (2), may not be unique. Examination of the physical considerations of the aircraft tracking control problem allows introduction of additional constraints, which reduce the DOFs to a feasible subset of the state and control space that contains the optimal solution. The minimization problem (3) is, thus, reduced to a simple procedure with a unique solution. Many possibilities exist for the choice of such additional constraints. The technique presented imposes the requirements of an (instantaneous) quasi-steady-state solution and a coordinated turn condition. This solution concept is outlined, and the detailed algorithm description follows in Sec. III.D.

The minimization of Eq. (3) occurs when the aircraft's main lifting surface orientation is optimal with respect to achieving the desired acceleration. More specifically, the x–z wind-axis plane must be rotated so that the desired acceleration vector $\boldsymbol{a}_{d_W}$ lies in that plane. The desired acceleration $\boldsymbol{a}_{d_W}$ includes gravitational effect

$$\boldsymbol{a}_{d_W} = C_{WV} \cdot \left(\boldsymbol{a}_{d_{\text{LVLH}}} - \boldsymbol{g}_{\text{LVLH}}\right) \tag{4}$$

where

$$C_{WV} = C_1(\phi_W) \cdot C_2\left(\theta_{W_0}\right) \cdot C_3\left(\psi_{W_0}\right)$$

where C_1, C_2, and C_3 are standard rotation matrices for roll, pitch, and yaw respectively[17]; ϕ_W, θ_W, and ψ_W are wind axis roll, pitch, and yaw attitude angles; and $\boldsymbol{g}_{\text{LVLH}} = [0\ 0\ g]^T_{\text{LVLH}}$, with g the acceleration due gravity.

The x–z wind-axis plane orientation is fixed by the bank angle ϕ_W of the aircraft. When examined from a stepwise, discrete viewpoint, this means simply that the aircraft must be placed in a quasitrimmed (or quasi-steady-state) flight condition in this desired orientation, with the corresponding states and controls such that 1) the achieved acceleration matches the desired acceleration [Eqs. (1)] and 2) moments about the center of gravity are zero [Eqs. (2)].

Given the aircraft's current flight condition (at time t_i), the quasitrimmed flight condition just described will be commanded at the next time step (time t_{i+1}). The assumption of a quasitrimmed flight condition implies that the body-axis angular accelerations are zero. This effectively adds the constraint

$$\dot{p} = \dot{q} = \dot{r} = 0$$

The final additional constraint, added to enable unique solution for the quasitrimmed states $\boldsymbol{x}$ and controls $\boldsymbol{u}$, is that all turning maneuvers are (instantaneously) steady and coordinated. This is used in calculation of the body-axis rates p, q, and r and effectively requires that the side force Y is zero [see Eq. (6) in Sec. III.D].

This method amounts to viewing the tracking of a trajectory as achieving a set of discrete, quasitrimmed flight conditions over time. Obviously this only refers to the feedforward component of the tracking control system; it is the function of the inner loop to control the continuously changing rates that will necessarily result from the dynamic tracking of a trajectory. For this reason, only the quasi-steady-states ϕ, u, v, and w are passed as tracking commands to the inner-loop controller (see Fig. 1).

D. Algorithm Description

The first operation in the trim solution loop is to select a bank angle ϕ to achieve the desired orientation of the aircraft. With reference to Eq. (4), a binary search procedure over the range $-90 < \phi_W < 90$ deg is used to iterate on ϕ_W until

$$\boldsymbol{a}_{d_W} = [\eta \quad 0 \quad \xi]^T \tag{5}$$

where η and ξ are arbitrary real numbers and the y_w axis component is zero, indicating that the x–z wind-axis plane has been optimally orientated with respect to the desired acceleration. The body-axis Euler angles ϕ, θ, and ψ are extracted using the solution for ϕ_W, from the coordinate transformation matrix relationship $C_{BV} = C_{BW} \cdot C_{WV}$.

Next, the body-axis rates p, q, and r are calculated. The requirement for steady, coordinated turns reduces the body-axis side-force component to zero, giving[17]

$$mg\sin\phi\cos\theta = m(ru - pw)$$

Body-axis rates in a steady turn are then given by

$$p = \min\left(-\frac{g\sin\phi\sin\theta}{u\cos\phi + w\tan\theta}, p_{\max}\right)$$
$$r = \min\left(\frac{g\sin\phi\cos\phi\cos\theta}{u\cos\phi + w\tan\theta}, r_{\max}\right) \tag{6}$$
$$q = \min[(r\tan\phi), q_{\max}]$$

If the required rates exceed allowable maximum values (at high bank angles, for example) they are limited, and the turn simply becomes uncoordinated, with body-axis side-force component nonzero.

Inverse solution of the nonlinear dynamics [Eqs. (1) and (2)] for the states α and β and the controls $\boldsymbol{u}$ forms the next stage of the trim function algorithm and is termed the states and controls iteration procedure. The six forces and moments X_W, Y_W, Z_W, L, M, and N may be written (in nondimensional form) as the sum of components due to each of the states and controls

$$C_A = C_{A_0} + C_{A_\alpha}\alpha + C_{A_\beta}\beta + C_{A_p}\hat{p} + C_{A_q}\hat{q} + C_{A_r}\hat{r} + C_{A_{\delta_e}}\delta_e + C_{A_{\delta_t}}\delta_t + C_{A_{\delta_a}}\delta_a + C_{A_{\delta_r}}\delta_r \tag{7}$$

where $A = X, Y, Z, L, M$, or N; $C_{A_{x/\delta}}$ are aerodynamic/control coefficients $[\partial C_A/\partial(x/\delta)]$; C_{A_0} are coefficient values when states and controls are zero; and $\hat{p} = pb/2V$, $\hat{q} = q\bar{c}/2V$, and $\hat{r} = rb/2V$, where $\bar{c}$ and b are wing chord and span lengths respectively.

The method used to obtain the aerodynamic and control coefficients $C_{A_{x/\delta}}$ in Eqs. (7) includes the full nonlinear mathematical model to accurately describe the aircraft dynamics over the entire flight envelope. The coefficients were calculated as detailed functions of the states and controls

$$C_{A_{x/\delta}} = f_C(V, \alpha, \beta, \boldsymbol{u}) \tag{8}$$

where the function f_C was based on extensive fifth-order curve fits of experimental wind-tunnel data and numerical flow analysis (also see Sec. IV.A).

Substitution of Eqs. (7) for the six forces and moments into Eqs. (1) and (2) yields (upon rearrangement) a system of matrix equations of the form

$$\left(\frac{m}{QS}\right)\cdot \boldsymbol{a}_{d_W} + \begin{bmatrix} C_{D_0} \\ -C_{Y_0} \\ C_{L_0} \end{bmatrix} + \begin{bmatrix} C_{D_{\delta_e}} & C_{D_{\delta_a}} & C_{D_{\delta_r}} & C_{D_p} & C_{D_q} & C_{D_r} \\ -C_{Y_{\delta_e}} & -C_{Y_{\delta_a}} & -C_{Y_{\delta_r}} & -C_{Y_p} & -C_{Y_q} & -C_{Y_r} \\ C_{L_{\delta_e}} & C_{L_{\delta_a}} & C_{L_{\delta_r}} & C_{L_p} & C_{L_q} & C_{L_r} \end{bmatrix} \cdot \begin{bmatrix} \delta_e \\ \delta_a \\ \delta_r \\ \hat{p} \\ \hat{q} \\ \hat{r} \end{bmatrix} = \begin{bmatrix} -C_{D_\alpha} & -C_{D_\beta} & -C_{D_{\delta_t}} \\ C_{Y_\alpha} & C_{Y_\beta} & C_{Y_{\delta_t}} \\ -C_{L_\alpha} & -C_{L_\beta} & -C_{L_{\delta_t}} \end{bmatrix} \cdot \begin{bmatrix} \alpha \\ \beta \\ \delta_t \end{bmatrix} \tag{9}$$

$$\begin{bmatrix} \frac{1}{QSb}(-(I_{yy} - I_{zz})qr) \\ \frac{1}{QS\bar{c}}\left(-I_{xz}(r^2)\right) \\ \frac{1}{QSb}(-I_{xz}(-qr)) \end{bmatrix} - \begin{bmatrix} C_{l_0} \\ C_{M_0} \\ C_{N_0} \end{bmatrix} - \begin{bmatrix} C_{l_\alpha} & C_{l_\beta} & C_{l_{\delta_t}} & C_{l_p} & C_{l_q} & C_{l_r} \\ C_{M_\alpha} & C_{M_\beta} & C_{M_{\delta_t}} & C_{M_p} & C_{M_q} & C_{M_r} \\ C_{N_\alpha} & C_{N_\beta} & C_{N_{\delta_t}} & C_{N_p} & C_{N_q} & C_{N_r} \end{bmatrix} \cdot \begin{bmatrix} \alpha \\ \beta \\ \delta_t \\ \hat{p} \\ \hat{q} \\ \hat{r} \end{bmatrix} = \begin{bmatrix} C_{l_{\delta_e}} & C_{l_{\delta_a}} & C_{l_{\delta_r}} \\ C_{M_{\delta_e}} & C_{M_{\delta_a}} & C_{M_{\delta_r}} \\ C_{N_{\delta_e}} & C_{N_{\delta_a}} & C_{N_{\delta_r}} \end{bmatrix} \cdot \begin{bmatrix} \delta_e \\ \delta_a \\ \delta_r \end{bmatrix} \tag{10}$$

which may be solved for $[\alpha, \beta, \delta_t]^T$ and $[\delta_e, \delta_a, \delta_r]^T$, respectively, using simple matrix inversion techniques. Equations (8–10) are then evaluated in an iterative manner until the solution for α, β, δ_e, δ_a, δ_r, and δ_t converges. The iteration comprises the following steps (cyclically): 1) evaluation of the coefficients [Eq. (8)], 2) solution of the force equations [Eq. (9)] for α, β, and δ_t, 3) re-evaluation of the coefficients [Eq. (8)], and 4) solution of the moment equations [Eq. (10)] for δ_e, δ_a, and δ_r.

Dividing the six force and moment equations into two sets of three equations for solution ensured that the force requirements were met by α, β, and δ_t, and the residual moment requirements were met by δ_e, δ_a, and δ_r.

Solution values for α, β, δ_t, δ_e, δ_a, and δ_r are then checked for feasibility according to the criteria discussed in the problem statement [Eq. (3)]. If the solution is inadmissable, the desired LVLH-axis acceleration $\boldsymbol{a}_{d_{\text{LVLH}}}$ is reduced in magnitude, and the entire process is repeated. Note that this rotates the corresponding desired wind-axis acceleration because the gravitational acceleration component remains constant. Maximum commanded accelerations were limited to ± 5 g in each of the three LVLH axis directions. This procedure is referred to as the state limitation loop and completes the structure of the algorithm.

This solution technique represents a constrained optimization in which specific knowledge of the system and dynamics has been included to reduce the search to a feasible subspace in which a unique, optimal solution can be found.

IV. Robust Control System Design and Analysis

This section describes the design and analysis of inner-loop controllers to track commands generated by the 6-DOF maneuver algorithm. A linear quadratic tracking (LQT) controller is used as a baseline for controller design comparisons. The vehicle models developed for flight simulation and controller design are also discussed, and the sources of error in these models are highlighted. The effect of uncertainty in the UAV aerodynamic and control derivatives on the stability and performance of the flight control system is examined. Finally, a robust controller design is developed to demonstrate that robust stabilization is achievable for "worst-case" model uncertainties.

A. Vehicle Models

Flight simulation of the UAV and control system analyses are performed using a high-fidelity nonlinear UAV model.[18] This model includes extensive wind-tunnel data and numerical flow analysis results, as well as detailed models of the vehicle mass properties, power plant, and operating environment. A multidimensional curve fit is used to provide a continuous model of the aerodynamic and control derivatives for a wide range of operating conditions. To facilitate linear tracking controller design and direct examination of the effect of parametric uncertainty, an accurate linear model has been developed from first principles.[19] This model incorporates details of the vehicle geometry, propulsion system, trim conditions, and aerodynamic derivatives and computes the linear system matrices directly. In general, the full nonlinear UAV model is used to represent the actual vehicle dynamics during simulation, whereas the linear model is used for controller design and analysis.

B. Sources of Model Uncertainty

The performance and stability robustness of any flight control system is highly dependent on the uncertainty in the model used for its design. Parametric uncertainty for the UAV is characterized and upper bounded in each of the aerodynamic and control derivatives. This, in turn, can be used to determine worst-case matrix perturbations in the linear model. To this end, analytical and experimental results have been evaluated for their contribution to model uncertainties. Details of the parametric uncertainty analysis are provided in Ref. 14, but are not the focus of this paper. Results showed uncertainties of within 10% for static stability derivatives, whereas dynamic derivative uncertainties ranged in the order of 10–45%. Dynamic derivatives, though, do not have a dominant effect on the

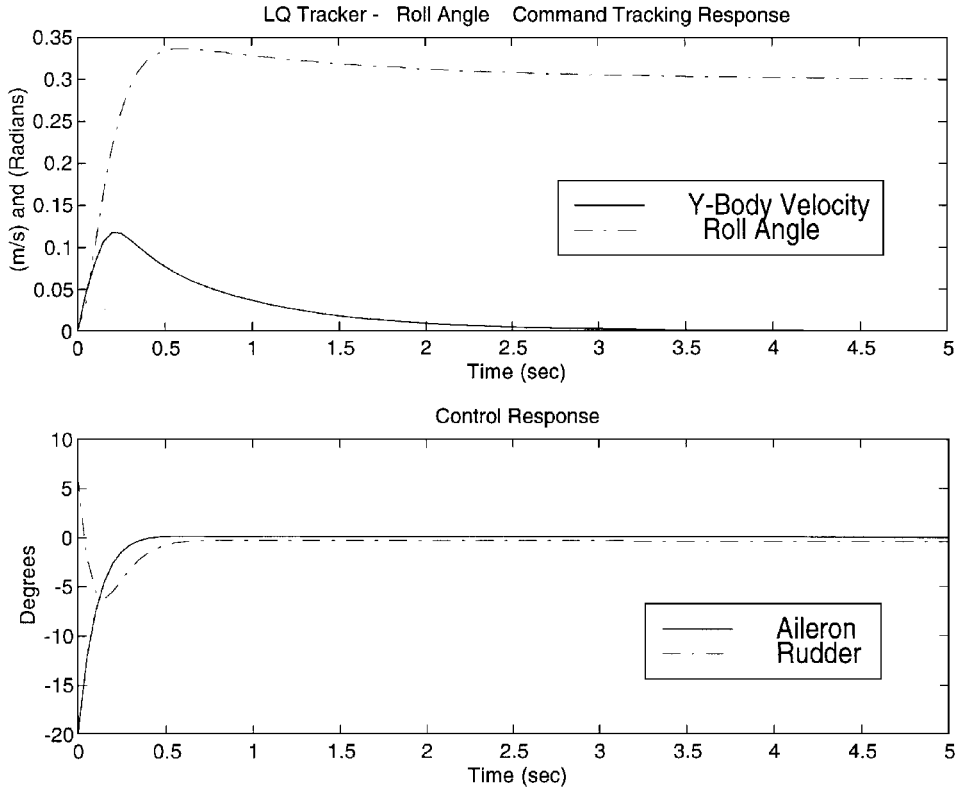

Fig. 2 Nominal step response, tracking roll angle.

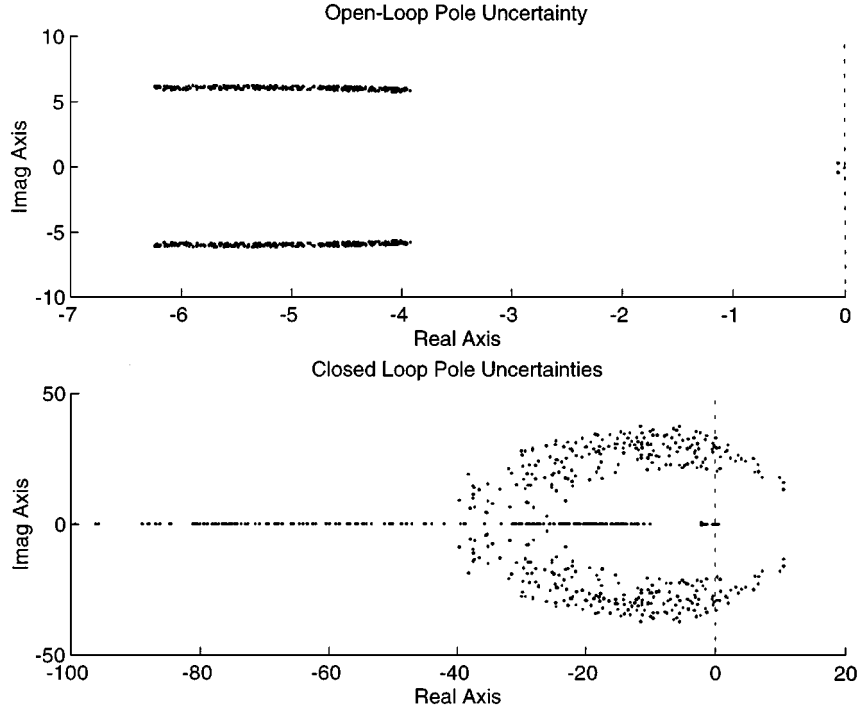

Fig. 3 Worst-case pole variations, nominal LQ design (longitudinal).

outcome of the linearized system matrices. Unmodeled dynamics are not specifically considered.

1. Linear Uncertainty Models

Whereas control system designs based on classical or modern control methods have inherent robustness properties, conventional measures of stability or performance can be very optimistic in the presence of model uncertainty. For this reason, the specific effect of parametric uncertainties on the structure of the linear model was examined. The range of possible parameter variations can be mapped to a set of possible system matrices through the augmented dynamic equations $\dot{\boldsymbol{x}}(t) = [A + \Delta A]\boldsymbol{x}(t) + [B + \Delta B]\boldsymbol{u}(t)$, where ΔA and ΔB represent all possible matrix perturbations consistent with the uncertainty in the original derivatives. Determining the maximum sizes of ΔA and ΔB requires an optimization over all possible parameter variations. This is simplified, however, by the algebraic nature of the influence of each coefficient on the relevant terms in the A and B matrices. The software developed for obtaining the worst-case perturbation matrices is documented in Ref. 19.

The effect of uncertainty in the aerodynamic and control derivatives can be visualized in terms of the characteristic mode shapes for the aircraft. Sampling across the range of possible ΔA and ΔB values (corresponding to a given set of parameter uncertainties), a scatter plot of resultant open- and/or closed-loop pole locations can be created. Figure 2 shows a step response for the nominal control system design (Sec. IV.C) and Fig. 3 provides an example scatter plot.

2. Wind Gust Disturbances

In the evaluation of closed-loop tracking performance, realistic disturbances have been included. The von Kármán gust model specified by MIL-SPEC-F-8785C (see Ref. 18) has been implemented in the simulation and is used for testing.

C. Linear Quadratic Tracker Design for Nominal Performance and Stability

For the baseline control system in this research, the linear quadratic (LQ) tracker configuration was used. The control law is of the form $\boldsymbol{u} = -K\boldsymbol{x}$, where K is defined by $R^{-1}B^T P$ and P is the solution to the algebraic Riccati equation

$$A^T P + PA - 2PBR^{-1}B^T P + Q = 0 \tag{11}$$

The system matrix A is an augmented matrix including additional states $\dot{\boldsymbol{z}} = \boldsymbol{y}_c - \boldsymbol{y}$, where $\boldsymbol{y}_c$ is the commanded output and $\boldsymbol{y} = C\boldsymbol{x}$ is the output vector. This amounts to adding integral action on the tracking errors of the system. The K matrix is partitioned into the terms K_r, K_y, and K_z, that is, the feedback gains on regulated states, tracking errors, and the integral of errors, respectively.

For simplicity, lateral and longitudinal controllers were developed separately. The conventional Q and R weighting matrices were adjusted to obtain good disturbance rejection, high damping, and a bandwidth that provides a fast response without saturation of control actuator limits or maximum rates. The tracking performance in following a step roll-angle command is shown in Fig. 2. Further details are given in Ref. 14. In general, the performance of both lateral and longitudinal controllers for the nominal UAV model are characterized by a short-response time, with little overshoot, and a fast-settling time (1.5 s for roll angle and 1.0 s for x-body velocity) with zero steady-state error. For sensible step commands, control actuator rates were also within specifications. The design point for this baseline LQT controller was a cruise flight condition, at 70-kn true airspeed and 1000-ft altitude, with the open- and closed-loop pole locations given in Table 1.

This LQ tracker design was taken as a nominal baseline controller with very good performance characteristics. The design serves as a useful best-performance yardstick for comparison purposes and was used in the following analysis to examine the potential adverse effects of specific parameter uncertainties on the stability and performance of the closed-loop system.

D. Analysis of Parametric Uncertainty

To characterize the relative importance of uncertainty in the aerodynamic and control derivatives, each of these parameters was varied over a specified range, and the resulting maximum linear model matrix perturbations ΔA and ΔB were obtained (see Sec. IV.B.1). For the nominal controller design of Sec. IV.C, the corresponding distribution of closed-loop pole locations was examined. This provided a useful test for the significance of individual parameter errors because the LQ design methodology is well known for having inherent robustness properties (60-deg phase margin and infinite gain margin).

The variation of open- and closed-loop poles was examined for all individual parameter uncertainties, to determine those which have the worst effect on closed-loop stability. From the pole-scatter diagrams, these parameters were readily identifiable as those with the ability to destabilize the closed-loop poles with the smallest relative uncertainty. These derivatives were then selected and used to construct a worst-case uncertainty configuration for the robust controller design (Sec. IV.E) and are given in Table 2.

E. Robust Control System Design

The approach taken for the development of robust tracking control laws was chosen for its ability to directly address the structure of the parameter variations in the system matrices. The details of the algorithm can be found in Ref. 20. In effect, the design comprises a nominal and robust contribution to the feedback gain matrix. The

Table 1 System pole locations

Open loop		Closed loop	
Longitudinal	Lateral	Longitudinal	Lateral
$-5.08 \pm 6.03i$	$-1.09 \pm 5.74i$	$-24.1 \pm 23.1i$	$-17.1 \pm 18.5i$
$-0.057 \pm 0.353i$	-11.04	$-2.04 \pm 0.323i$	$-9.49 \pm 3.32i$
	-0.069	-1.41	-1.40
		-0.017	-0.820

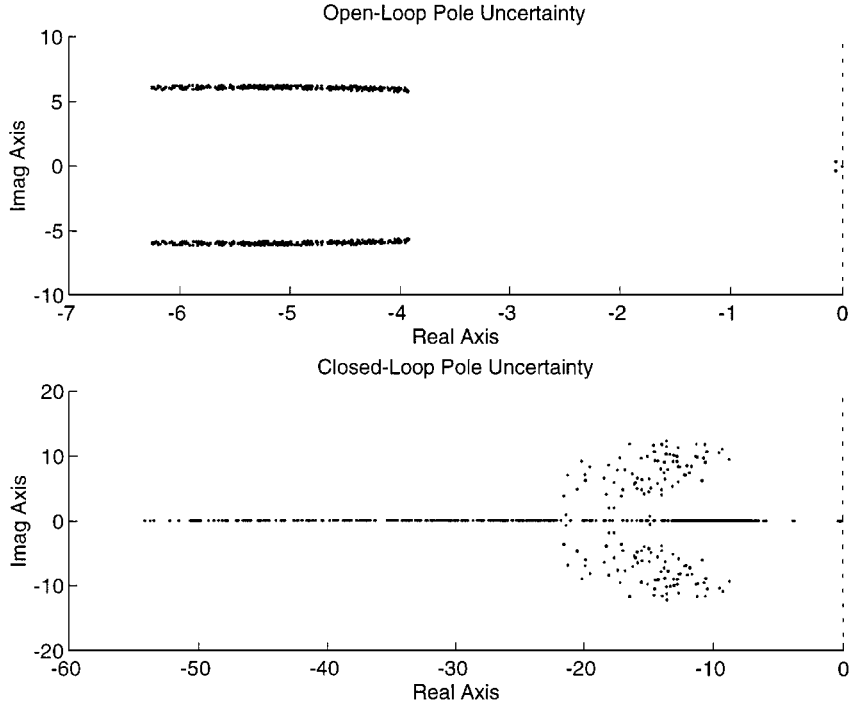

Fig. 4 Worst-case pole variations, robust Lyapunov design (longitudinal).

Table 2 Worst-case derivative uncertainties

Derivative	Uncertainty, %
Longitudinal	
C_L	50
C_{L_α}	50
$C_{L_{\delta t}}$	150
$C_{M_{\delta e}}$	50
$C_{M_{\delta t}}$	50
Lateral	
$C_{Y_{\delta r}}$	120
C_{l_p}	100
$C_{l_{\delta a}}$	90
$C_{l_{\delta r}}$	175
$C_{N_{\delta r}}$	70

system is assumed to be of the form $\dot{\boldsymbol{x}}(t) = [A_0 + \Delta A(\boldsymbol{r})]\boldsymbol{x}(t) + [B_0 + \Delta B(\boldsymbol{s})]\boldsymbol{u}(t)$, where $\boldsymbol{r}$ and $\boldsymbol{s}$ are vectors of the uncertain parameters. The dynamics are augmented by the state equation $\dot{\boldsymbol{z}}(t) = C_0\boldsymbol{x} - \boldsymbol{y}_c$, and the control law has the form $\boldsymbol{u}(t) = (K_0 + K_1)\boldsymbol{x}'$, where $\boldsymbol{x}' = [\boldsymbol{x}\ \boldsymbol{z}]^T$. It is desired to have the output track the commanded input:

$$\lim_{t\to\infty} \boldsymbol{y}(t) = \boldsymbol{y}_c$$

The feedback matrix K_0 can be any stabilizing gain matrix for the augmented tracking system, and the LQ tracker design (Sec. IV.C) satisfies this description. The robust controller is designed through iterative solution of a Lyapunov equation that involves the nominal closed-loop system. An inner loop performs a search over the parameter space to determine if the closed-loop poles are robustly

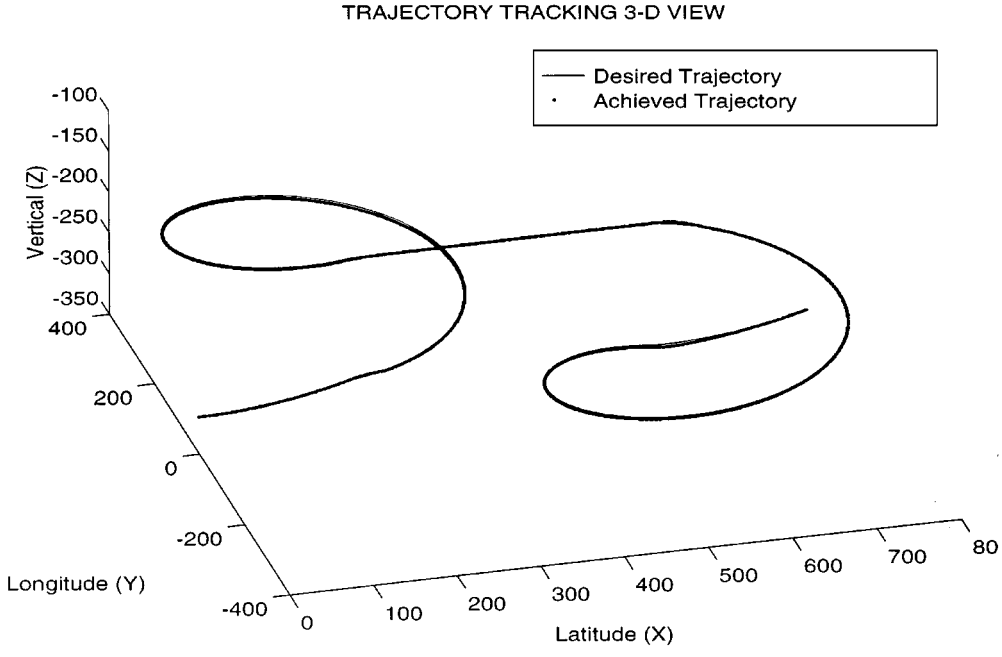

Fig. 5 Case 1: nominal tracking performance.

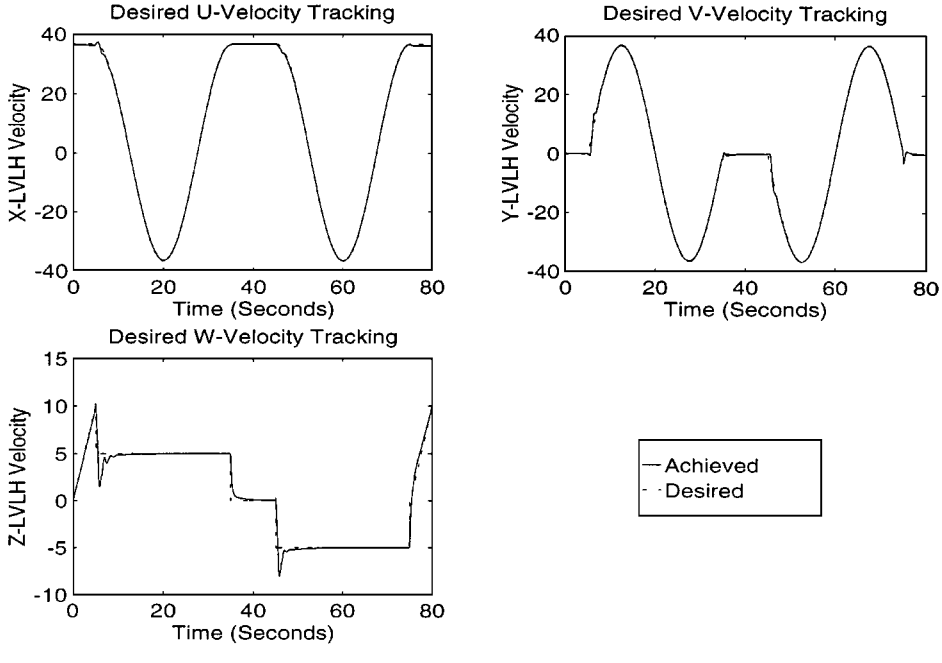

Fig. 6 Case 1: nominal LVLH velocity tracking.

stabilized. A single gain parameter is adjusted until the control law stabilizes any system matrices in the parameter set. The advantage of this approach is that the structure of the uncertainty is addressed directly by the computation of the maximum real part of the closed-loop poles for any parameter values in the uncertainty set. The result, however, can be conservative, and it may be possible to find a robust stabilizing control law with a lower gain.

The advantage of the robust controller design is well demonstrated by Figs. 3 and 4, which show the open- and closed-loop pole distribution for the longitudinal worst-case derivative uncertainties listed in Table 2. Whereas the nominal controller (Fig. 3) results in a potentially unstable design, the robust controller (Fig. 4) is able to stabilize the system. The result for lateral control is analogous, and the details are given in Ref. 14.

Although these results demonstrate that significant uncertainty can be accommodated in the aerodynamic and control coefficients, it is important to note that stability has been tested only for small perturbations from the trim flight condition. For large magnitude maneuvers, these results would be optimistic because the trajectory could require deviations from the flight envelope for which this linear state-space analysis is valid. In addition, the issue of robust performance has not been addressed, and the ability of this controller to track maneuver commands can be significantly degraded in the presence of uncertainty. These issues motivate current research, which is aimed at developing a robust, nonlinear 6-DOF maneuver autopilot, which eliminates the need for a linearized inner-loop controller.

It should also be noted that methods such as quantitative feedback theory (QFT),[21,22] which are capable of attaining robust performance specifications as well as stabilization, would be applicable as inner-loop controllers here.

F. Limitations

Whereas the 6-DOF feed-forward maneuver autopilot aids greatly in overcoming plant nonlinearities, the tracking control system as presented is limited due to the utilization of only a single LQT design as the inner-loop controller. Maneuvers are, thus, limited to those

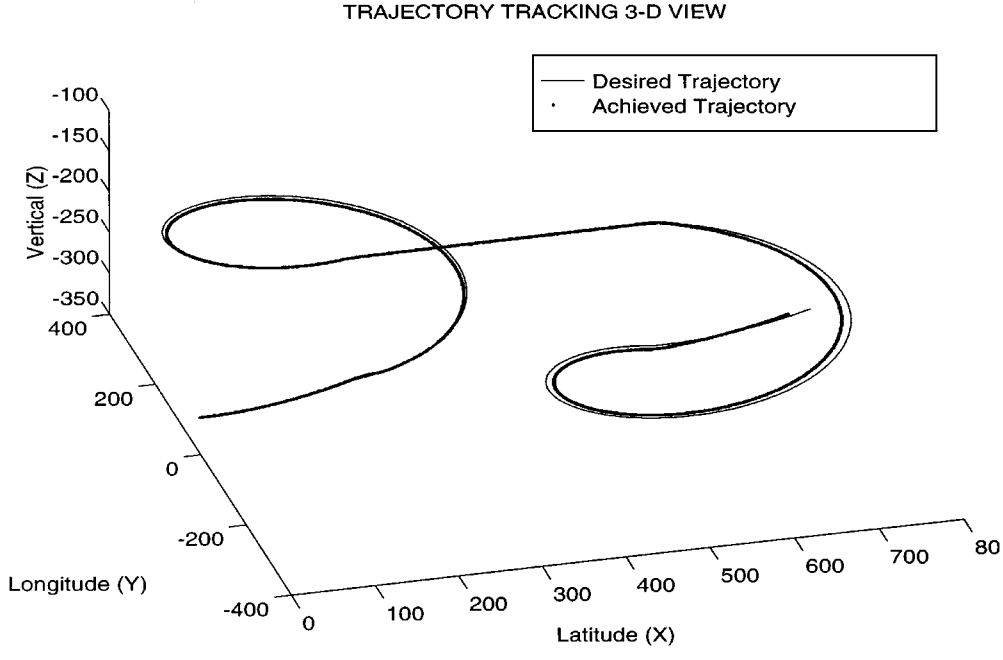

Fig. 7 Case 2: tracking performance without feedforward.

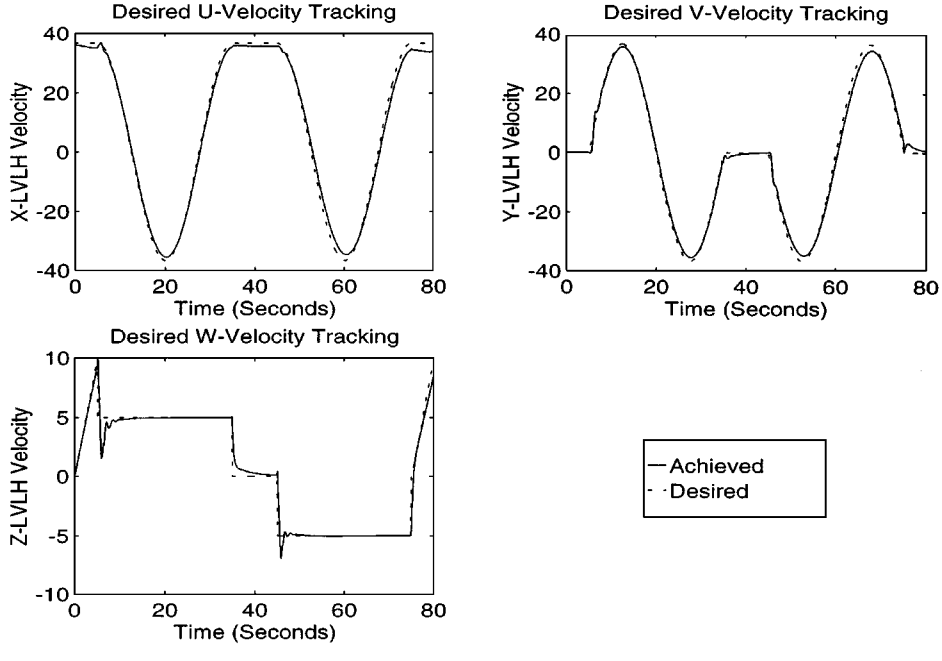

Fig. 8 Case 2: LVLH velocity tracking without feedforward.

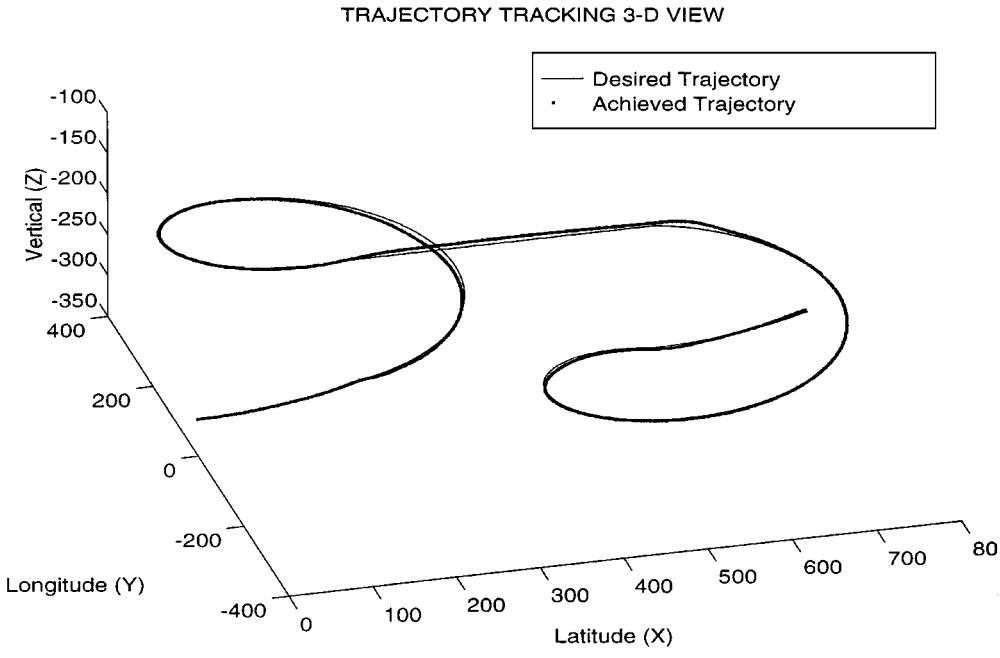

Fig. 9 Case 3: tracking performance with gusts.

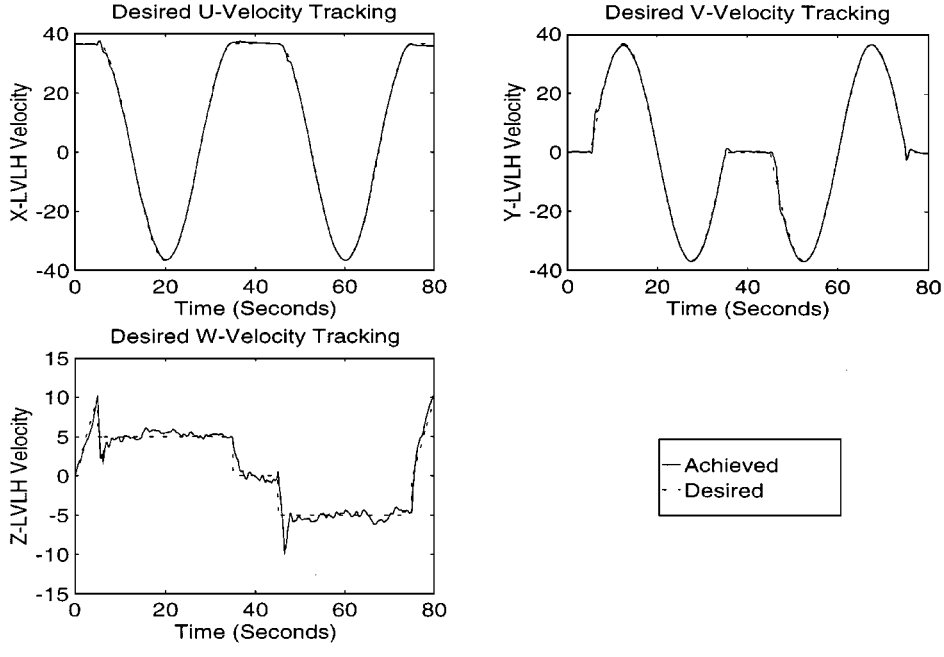

Fig. 10 Case 3: LVLH velocity tracking with gusts.

in which the velocity does not change by more than approximately 8 kn from the cruise (design) value. At very least, several LQT controllers designed at different velocities would be required to adequately cover the entire maneuver envelope for the UAV.

V. Maneuver Tracking

The maneuver tracking examples given in this section were based on simulation results for UAV *Ariel*. The maneuver defined as the desired trajectory in the following results was representative of maneuvers that the aircraft would be expected to handle during autonomous flight. The desired trajectory consisted of the following sequence: 1) a wings-level accelerated descent at 2 ms^{-2}, 2) a 360-deg descending right turn with a constant descent rate of 5 ms^{-1} (~1000 ft/min) and a turn rate of 12 deg/s, 3) a straight and level segment of 10-s duration, 4) a 360-deg ascending left turn with a constant ascent rate of 5 ms^{-1} (~1000 ft/min) and a turn rate of 12 deg/s, and 5) a wings-level accelerated descent at 2 ms^{-2}.

This combination of separate maneuver segments provided examples of straight and level, climbing, descending, and turning flight, whereas the transitions between the segments provided examples of pull-ups and push-overs. This trajectory was used for three test cases, the results of which are presented here. In each of the three cases, the UAV entered the maneuver from a cruise flight condition of 70-kn true airspeed at an altitude of 1000 ft.

A. Case 1: Nominal Tracking System

Case 1 consisted of the nominal tracking system (6-DOF trim algorithm coupled with LQ inner-loop controller). The results for case 1 are shown in Figs. 5 and 6. Excellent tracking performance was exhibited by the nominal system, as seen in Fig. 5, with a maximum position error of 3.6 m. The abrupt transitions required in

z-wise LVLH velocity (W velocity) between maneuver segments are obvious in Fig. 6, and result in damped transients with approximate durations of 5–6 s. These transients also appear in the x- and y-wise velocity components to a lesser extent, but are insignificant in effect on the maneuver tracking performance.

B. Case 2: Tracking System Without Feedforward Control

Case 2 consisted of the nominal tracking system used in case 1 but with an important modification. The feedforward commands from the 6-DOF trimming function were disconnected, leaving the control commands to be provided by the inner-loop controller only. Tracking performance was noticeably degraded, as seen in Fig. 7, with the maximum position error increasing to 25.8 m. The lag exhibited due to loss of feedforward control was also visible through extended transients (~10 s) and poorer overall tracking in the LVLH-axis velocity components (Fig. 8) as compared with the nominal system (Fig. 6). This highlights the importance of the feedforward control component in successful high-performance maneuver tracking.

C. Case 3: Nominal Tracking System with Disturbances

Case 3 comprised the nominal tracking system used in case 1 with the introduction of disturbances (in the form of gusts) for the duration of the tracking maneuver. The von Kármán gust model (Sec. IV.B.2) was used, with a realistic moderate turbulence level of average strength 10 ms^{-1} (~20 kn). Although tracking performance (Fig. 9) was degraded in comparison with the nominal system (Fig. 5), it remained satisfactory in the presence of adverse wind conditions. The maximum position error was 6.1 m. As is normally the case, the most significant effect of the turbulence was on the z-wise velocity component (Fig. 10).

VI. Conclusion

This paper has presented a high-performance maneuver autopilot capable of accurate trajectory following in the presence of nonlinear aircraft dynamics and parametric uncertainty. The approach is based on a 6-DOF nonlinear trimming algorithm coupled with a robust inner-loop controller. The effect of uncertainty in vehicle aerodynamic and control derivatives on closed-loop stability was analyzed, and it was shown that a robust inner-loop controller could be designed for expected levels of modeling error. The system was demonstrated through the use of a high-fidelity model of UAV *Ariel*. Simulated flights along a representative trajectory illustrated the importance of feedforward control in achieving good tracking performance. Successful results were obtained for a realistic flight with significant wind gust disturbances, suggesting that this approach may be suitable for the development of a fully autonomous flight vehicle.

References

[1]Wertz, V. J., De Souza, C. E., Loveridge, M. J., Feik, R. A., and Martin, C. A., "Design of a Manoeuvre Autopilot," *Proceedings of the Australian Aviation Symposium* (Canberra, Australia), National Conf. Publication No. 87/16, Inst. of Engineers Australia, Barton, ACT, Australia, 1987, pp. 25–29.

[2]Gao, C., and Hess, R. A., "Inverse Simulation of Large-Amplitude Aircraft Maneuvers," *Journal of Guidance, Control, and Dynamics*, Vol. 16, No. 4, 1993, pp. 733–737.

[3]Hess, R. A., Gao, C., and Wang, S. H., "Generalized Techniques for Inverse Simulation Applied to Aircraft Maneuvers," *Journal of Guidance, Control, and Dynamics*, Vol. 14, No. 5, 1991, pp. 920–926.

[4]Jung, Y. C., and Hess, R. A., "Precise Flight-Path Control Using a Predictive Algorithm," *Journal of Guidance, Control, and Dynamics*, Vol. 14, No. 5, 1991, pp. 936–942.

[5]Gibbens, P. W., and Goodwin, G. C., "Robustness Issues in Manoeuvre Autopilot Design," *Proceedings of the Australian Aeronautical Conference* (Melbourne, Australia), National Conf. Publication No. 89/14, Inst. of Engineers Australia, Barton, ACT, Australia, 1989, pp. 38–42.

[6]Azam, M., and Singh, S. N., "Invertibility and Trajectory Control for Nonlinear Maneuvers of Aircraft," *Journal of Guidance, Control, and Dynamics*, Vol. 17, No. 1, 1994, pp. 192–200.

[7]Gopalswamy, S., and Hedrick, J. K., "Robust Adaptive Nonlinear Control of High Performance Aircraft," *Proceedings of the 10th American Control Conference*, Inst. of Electrical and Electronics Engineers, New York, 1991, pp. 1279–1284.

[8]Menon, P. K. A., Badgett, M. E., Walker, R. A., and Duke, E. L., "Nonlinear Flight Test Trajectory Controllers for Aircraft," *Journal of Guidance, Control, and Dynamics*, Vol. 10, No. 1, 1987, pp. 67–72.

[9]Menon, P. K. A., Walker, R. A., and Duke, E. L., "Flight-Test Maneuver Modeling and Control," *Journal of Guidance, Control, and Dynamics*, Vol. 12, No. 2, 1989, pp. 195–200.

[10]Sentoh, E., and Bryson, A. E., "Inverse and Optimal Control for Desired Outputs," *Journal of Guidance, Control, and Dynamics*, Vol. 15, No. 3, 1992, pp. 687–691.

[11]Meyer, G., and Cicolani, L., "A Formal Structure for Advanced Automatic Flight Control Systems," NASA TN-D-7940, May 1975.

[12]Smith, G. A., and Meyer, G., "Aircraft Automatic Flight Control System with Model Inversion," *Journal of Guidance, Control, and Dynamics*, Vol. 10, No. 3, 1987, pp. 269–275.

[13]Weiss, J., Eterno, J., Grunberg, D., Looze, D., and Ostroff, A., "Investigation of an Automatic Trim Algorithm for Restructurable Aircraft Control," *Proceedings of the IEEE 1986 National Aerospace and Electronics Conference, NAECON 1986* (Dayton, OH), Vol. 2, Inst. of Electrical and Electronics Engineers, New York, 1986, pp. 400–406.

[14]Chamitoff, G. E., Wong, K. C., Newman, D. M., and Boyle, D. P., "Autonomous Guidance and Robust Control for a Remotely Piloted Vehicle," Aeronautical Engineering, TR Aero 9802, Univ. of Sydney, Sydney, Australia, Feb. 1998,

[15]Chamitoff, G. E., "Real-Time Autonomous Guidance for Self-Piloted Vehicles," *Proceedings of the 2nd Pacific International Conference on Aerospace Science and Technology*, Melbourne, Australia, 1995.

[16]Ho, L. C., "Mission and Trajectory Planning for Autonomous Operations of a Remotely Piloted Vehicle," B.E. Thesis, Dept. of Aeronautical Engineering, Univ. of Sydney, Sydney, Australia, Nov. 1994.

[17]Etkin, B., *Dynamics of Atmospheric Flight*, Wiley, New York, 1972, Chaps. 4 and 5.

[18]Newman, D. M., and Wong, K. C., "Six Degree of Freedom Flight Dynamic and Performance Simulation of a Remotely Piloted Vehicle," Aeronautical Engineering, TR Aero 9301, Univ. of Sydney, Sydney, Australia, June 1993.

[19]Boyle, D. P., "Robust Nonlinear Control for Autonomous Manoeuvre Tracking," Ph.D. Thesis, Dept. of Aeronautical Engineering, Univ. of Sydney, Sydney, Australia (to be completed 1998).

[20]Schmitendorf, W. E., and Barmish, B. R., "Robust Asymptotic Tracking for Linear Systems with Unknown Parameters," *Automatica*, Vol. 22, No. 3, 1986, pp. 355–360.

[21]Horowitz, I., "Survey of Quantitative Feedback Theory (QFT)," *International Journal of Control*, Vol. 53, No. 2, 1991, pp. 255–291.

[22]Hess, R. A., and Gorder, P. J., "Quantitative Feedback Theory Applied to the Design of a Rotorcraft Flight Control System," *Journal of Guidance, Control, and Dynamics*, Vol. 16, No. 4, 1993, pp. 748–753.